Preprints of the 19th World Congress
The International Federation of Automatic Control
Cape Town, South Africa. August 24-29, 2014

Vibration Suppression for Angular Transmission Errors in Harmonic Drive Gearings and Application to Industrial Robots

Makoto Iwasaki * **Hiroyuki Nakamura** *

* *Department of Comp. Sci. & Eng., Nagoya Institute of Technology, Nagoya, JAPAN (e-mail: iwasaki@nitech.ac.jp).*

Abstract: This paper presents a vibration suppression approach for precision positioning mechanisms including harmonic drive gearings (HDGs), using a variable notch filter to suppress mechanical vibrations due to angular transmission errors (ATEs) in HDGs. Mechanisms with HDGs excite resonant vibrations, especially in the condition that the frequency of synchronous components of ATE correspond to the critical mechanical resonant frequency. In the proposed approach, therefore, a variable notch filter with free parameters of frequency and damping is designed to suppress the resonant vibrations during transient response, considering the sensitivity characteristics of the feedback system. The proposed approach has been applied to motion control of an actual industrial 6-axis robot and verified by numerical simulations and experiments.

1. INTRODUCTION

Varieties of industrial robots have been widely applied to extensive factory automation fields, where the fast and precise point-to-point and/or tracking control performance of end effectors should be essential to provide the high productivity and quality in the manufacturing. In order to ensure the requirements, a wide variety of control approaches have been already proposed, e.g., state-feedback control, model-based feedforward control, iterative learning control, and adaptive control, to compensate for the deterioration factors, such as resonant vibrations due to the flexibility of joints, nonlinearities, variations and/or uncertainties in mechanical parameters, and interference force between axes (Spong et al. [1987], Spong et al. [2005], Khorasani [1992], Miyazaki et al. [2002], Kennedy et al. [2005], Bona et al. [2006]).

Actuators in robot axes are generally controlled in a semi-closed control manner due to the mechanical constraints, that is, motor states (displacement and/or velocity) for each axis are directly detected and controlled by sensors on the motor shafts. The independent controller for each axis, therefore, is designed on the basis of a linear 2-inertia system composed of a motor, a reduction gear, and an arm. However, since reduction gears inherently possess nonlinear components known as ATEs due to structural errors and flexibility, the ideal control accuracy corresponding to the apparent resolution cannot be essentially attained at the end effector of robot manipulator (Tuttle et al. [1996], Ghorbel et al. [2001], Godler et al. [2001]). One of ATEs, called "synchronous component", is a periodical angular transmission error due to the structural errors in manufacturing process of gears, which is synchronous to the rotation of gearing. Resonant vibrations, therefore, are generated when the frequency of synchronous components corresponds to the mechanical resonance one of axis. Since the resonance frequencies are generally exist at around the control bandwidth of each axis, a controller design considering the vibration suppression should be indispensable for the robot operations.

Under the background above, this research especially focuses on the suppression control for resonant vibrations due to the periodical disturbance of synchronous component in HDGs, which deteriorate the control performance (Iwasaki et al. [2009], Yamamoto et al. [2010]). In the controller design, the synchronous component is modeled and, then, the resonant vibrations are analyzed using an actual 6-axis industrial robot. Based on the analyses, a feedback compensator to suppress the vibration is designed from a viewpoint of the loop-shaping framework (Seki et al. [2009]), where a variable notch filter is applied to reduce the sensitivity gain for the synchronous component. The proposed control has been verified by experiments using the actual industrial robot.

2. 6-AXIS ROBOT CONTROL SYSTEM

2.1 Configuration of Robot System

Fig. 1 illustrates a schematic diagram of a typical 6-axis industrial robot. Each axis can be modeled as a 2-inertia system composed of a servo motor as an actuator, a HDG as a reduction gear, and an arm, where a semi-closed controller is applied to the each actuator using the detected motor angle by a sensor on the motor shaft. In the robot system as an experimental setup, a triaxial acceleration sensor is attached on the tip of robot to evaluate the vibration suppression performance.

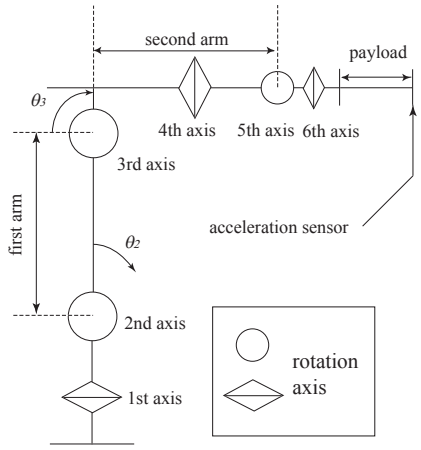

Fig. 1. Schematic diagram of 6-axis industrial robot.

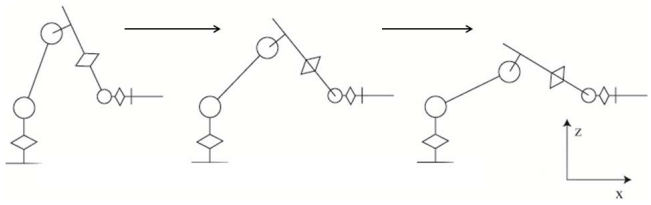

Fig. 2. Schematic diagram of line motion.

2.2 Target Control Specifications

In the research, a line motion in the X-axis direction as shown in Fig. 2 is evaluated as a target robot motion profile, where the 2nd, 3rd and 5th axes are manipulated. Since motion behaviors of the 2nd and 3rd axes especially affect the control performance, the modeling and controller design for the axes should be indispensable subjects in the research.

One of typical control specifications is given that the resonant vibration at the robot tip due to the ATEs should be suppressed within ±0.05 mm. Here, the acceleration signal at the tip is alternatively evaluated by converting the equivalent displacement, where the vertical (Z-axis direction) acceleration signal is measured to evaluate the suppression performance.

3. MATHEMATICAL MODELING OF AXIS AS 2-INERTIA SYSTEM

3.1 Plant Modeling by 2-Inertia System

Plant system for each axis can be mathematically modeled as a 2-inertia system for the motor and arm connected by the HDG. Fig. 3 shows a block diagram of the plant with a control loop as a semi-closed feedback control in motor side, where J_m: motor inertia, D_m: viscous friction of motor, J_l: arm inertia, D_l: viscous friction of arm, K_g: stiffness of gear, D_g: damping coefficient of gear, N: reduction ratio of gear, θ_m: motor angular position, θ_l: arm angular position, τ_{ref}: motor torque reference, θ_{ref}: motor angular position reference, $K(s)$: P-PI feedback compensator (proportional for position, proportional and integral for velocity), and ATE model: synchronous component model for ATE, respectively. In the mathematical model,

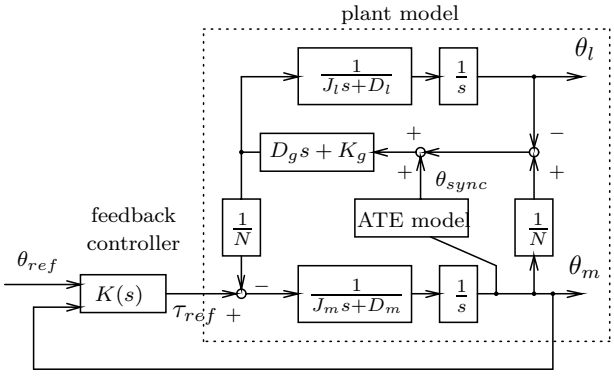

Fig. 3. Block diagram of 2-inertia system for each axis.

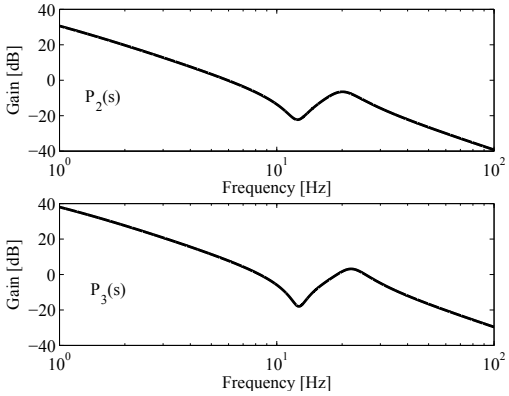

Fig. 4. Example of frequency characteristics of motor angular position for torque reference in 2nd and 3rd axes.

the synchronous component θ_{sync} of ATEs is handled as an angular disturbance for the torsional angle of $(\theta_m/N - \theta_l)$. K_g and D_g are identified by experimental frequency characteristics of motor angle for torque reference. Friction and gravity are included in the actual simulator, where the corresponding parameters are calculated by geometric data and/or measured by experiments (Kim et al. [2012]).

Fig. 4 shows an example of frequency characteristics of 2-inertia model for the 2nd and 3rd axes, where upper figure represents a linear plant characteristic of the 2nd axis $P_2(s)$ and lower figure represents that of the 3rd axis $P_3(s)$. From the figures, each plant apparently includes the resonant vibration frequency at around 22 Hz and anti-resonant frequency at around 12 Hz.

3.2 Modeling for Synchronous Component of ATEs

The angular transmission error θ_{ATE} is generally defined as follows, by the motor angular position θ_m, the load (arm) angular position θ_l, and the gear ratio N.

$$\theta_{ATE} = \theta_l - \frac{\theta_m}{N} \tag{1}$$

The synchronous component θ_{sync} of ATE is basically caused by kinematic errors in teeth of a flex spline and a circular spline, and assembling errors in shaft of gearing and load, which is synchronous to the relative rotation of a wave generator, a flex spline, and a circular spline. Fig. 5 shows an example waveform of θ_{sync} for θ_l, where vertical

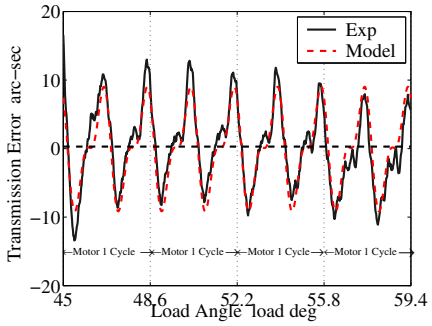

Fig. 5. Example of waveforms of synchronous component of ATE.

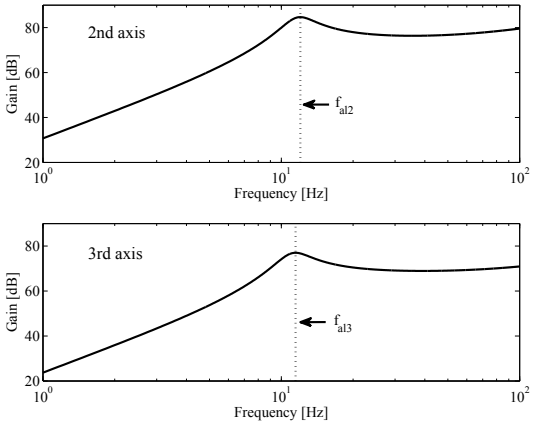

Fig. 6. Gain characteristics of load acceleration for synchronous component in 2nd and 3rd axes.

dotted lines represents one cycle of motor rotation. From the waveform, θ_{sync} is mainly composed of the 2nd and 4th order harmonics for θ_m. In the robot system, the 2nd and 4th order harmonics of θ_{sync} becomes the dominant factor to deteriorate the control performance. The synchronous component, therefore, can be mathematically formulated by the following periodical pulsation for θ_m:

$$\theta_{sync} = A_2 \cos(2\theta_m + \phi_2) + A_4 \cos(4\theta_m + \phi_4), \quad (2)$$

where A_n and ϕ_n are the amplitude and phase for nth component. The broken line in Fig. 5 is an example of fitted model for θ_{sync} by (2).

The frequency f_{sync} of θ_{sync}, on the other hand, can be given as follows:

$$f_{sync} = k f_m, \quad (3)$$

where f_m is the frequency of motor velocity and k is the order of θ_{sync}.

In the Fig. 3, the transfer function $G_{al}(s)$ of the arm acceleration $a_l = \ddot{\theta}_l$ for θ_{sync} can be defined as the following sensitivity function.

$$G_{al}(s) = \frac{a_l}{\theta_{sync}} \quad (4)$$

Fig. 6 shows gain characteristics of $G_{al}(s)$ in the 2nd and 3rd axes. From each figure, since $G_{al}(s)$ has a peak gain at around $f_{al} = 12$ Hz, the resonant vibration at the

Table 1. Relation between peak frequency of G_{al} and resonant velocity.

axis		2nd	3rd
gain peak frequency of G_{al}	f_{al} [Hz]	11.84	11.45
excitation velocity of 2nd order synchronous component	f_{m2} [rps]	5.92	5.72
excitation velocity of 4th order synchronous component	f_{m4} [rps]	2.96	2.86

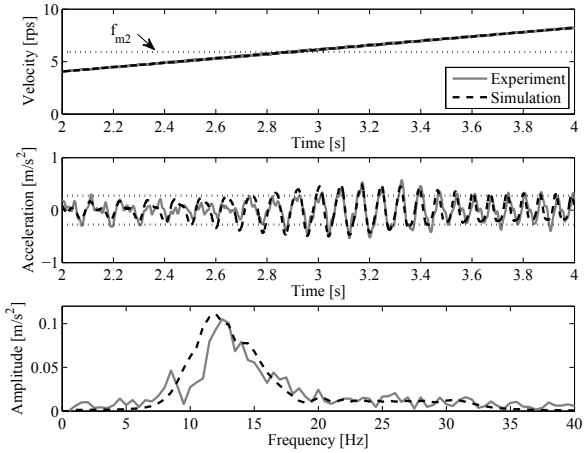

(a) 2nd order harmonics of θ_{sync}.

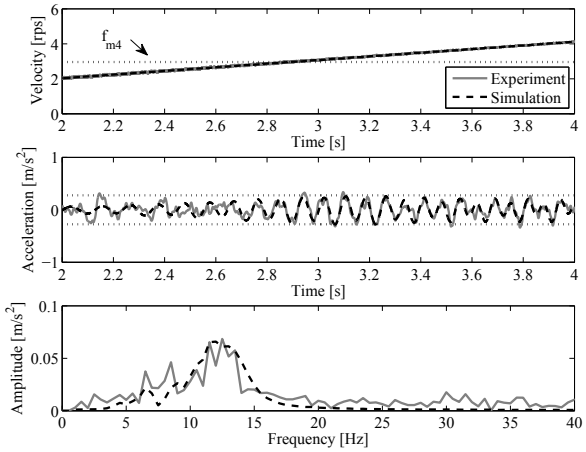

(b) 4th order harmonics of θ_{sync}.

Fig. 7. Example response waveforms under constant acceleration motion in 2nd axis.

end effector is generated under the condition that f_{sync} corresponds to f_{al}. Table 1 lists the excited frequency by (3) of arm side vibration for each axis.

In order to formulate the mathematical model of θ_{sync}, the angular transmission error between motor and arm angular position should be directly measured by experiments and, then, the parameters can be identified by fitting the spectrum of the experimental waveforms (Iwasaki et al. [2009]). However, since the arm angular position for each axis cannot be directly measured in the actual robot, the parameters should be indirectly identified by using vibration waveforms of the tip acceleration. At first, the motor is driven under a constant acceleration to pass through f_{m2} and f_{m4} in Table 1. Based on the experimental results under the constant acceleration, the parameters of θ_{sync} can

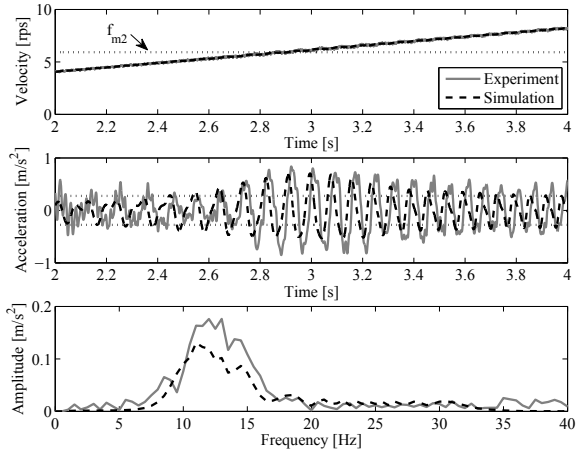

(a) 2nd order harmonics of θ_{sync}.

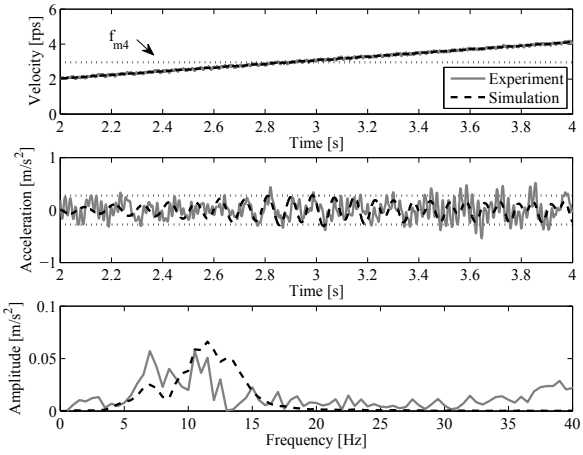

(b) 4th order harmonics of θ_{sync}.

Fig. 8. Example response waveforms under constant acceleration motion in 3rd axis.

Table 2. Parameters of synchronous component.

axis		2nd	3rd
A_2	[arc-sec]	5	10
ϕ_2	[deg]	222	262
A_4	[arc-sec]	3	5
ϕ_4	[deg]	126	306

be identified to fit between experiments and mathematical model of (2). Figs. 7 and 8 show example waveforms for the modeling procedures, where Fig. 7 indicates waveforms for the 2nd and 4th order harmonics of θ_{sync} in the 2nd axis, and Fig. 8 indicates the ones in the 3rd axis. In these figures, the top shows the motor velocity, the middle shows the acceleration of end effector, the bottom shows frequency analyses of the acceleration, solid lines represent the experimental results, broken lines represent the responses of mathematical model, and dotted horizontal lines in the middle indicate the reference acceleration. Table 2 lists the identified parameters of θ_{sync} in (2).

From these results, the simulator can well-reproduce the resonant vibration caused by θ_{sync}, while the resonant vibrations caused by the 2nd order harmonics in both axes are especially dominant to excite the vibration. In the following, therefore, the controller are especially designed paying attention to the 2nd order harmonics of θ_{sync}.

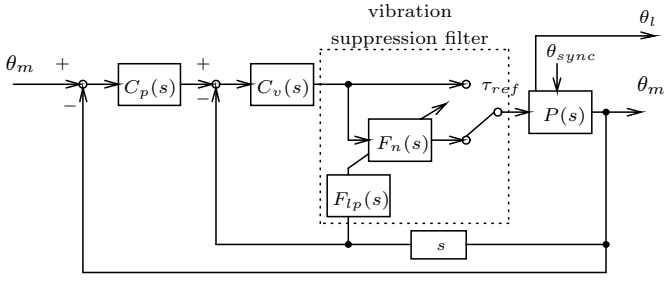

Fig. 9. Block diagram of vibration suppression control.

4. CONTROLLER DESIGN CONSIDERING VIBRATION SUPPRESSION

4.1 Guideline for Vibration Suppression Controller

In the research, the target control accuracy is set as of A_{acc} ($= \pm 0.05$ mm) at the end effector, while the acceleration signal is measured by the sensor at the tip of robot in the experiments. In order to suppress the tip vibration due to θ_{sync} within ± 0.05 mm, a loop-shaping is applied to the feedback control system. In the design, the gain of $G_{al}(s)$ should satisfy the following constraint.

$$|G_{al}(j\omega)| \leq 20\log_{10}\frac{A_{acc}}{A_n}\omega^2 \tag{5}$$

Since the 2nd order harmonics of θ_{sync} especially affects the control performance from the examinations in Figs. 7 and 8, the feedback compensator can be designed paying attention to reduce the gain of $G_{al}(s)$ as $A_n = A_2$ in (5).

4.2 Design of Variable Notch Filter

Fig. 9 shows a block diagram of control system considering the vibration suppression, where $P(s)$: plant, $C_p(s)$: proportional compensator for angular position, $C_v(s)$: proportional-integral compensator for angular velocity, $F_n(s)$: loop-shaping filter, and $F_{lp}(s)$: lowpass filter to remove sensor noises. $F_n(s)$ is designed as the following notch filter to reduce the peak gain of $G_{al}(s)$.

$$F_n(s) = \frac{s^2 + 2\zeta_{rn}\omega_{rn}s + \omega_{rn}^2}{s^2 + 2\zeta_{rd}\omega_{rd}s + \omega_{rd}^2} \cdot \frac{\omega_{rd}^2}{\omega_{rn}^2} \tag{6}$$

In order to improve the phase delay at around the frequency of notch filter, the angular frequencies ω_{rn} and ω_{rd} are set as follows (Seki et al. [2009]):

$$\omega_{rd} = \omega_{rn} + \omega_d, \tag{7}$$

where ω_d is the offset angular frequency, ω_{rn} is synchronized with f_m, and ω_{rn} is set as kf_m.

From a viewpoint of the feedback system stability, however, $F_n(s)$ cannot be applied in all angular velocity range. Therefore, $F_n(s)$ is switched as a variable filter as shown in Fig. 9 at around the frequency of peak gain in $G_{al}(s)$, where the parameters are designed to ensure the system stability and to satisfy (5). Table 3 lists the designed

Table 3. Designed parameters of variable notch filter.

axis		2nd	3rd
ω_d	[rad/s]	$2\pi \times 0.5$	$2\pi \times 0.7$
ζ_{rn}		0.028	0.036
ζ_{rdth}		0.1	0.1
k		2	
f_s	[rps]	4	
f_e	[rps]	9	

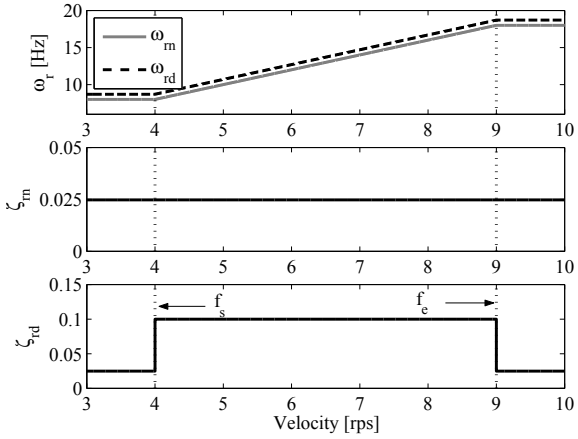

Fig. 10. Variable parameters in notch filter.

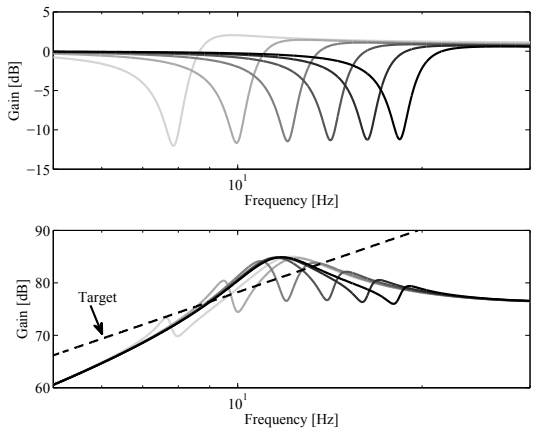

Fig. 11. Gain characteristics of notch filter and $G_{al}(s)$.

parameters, while Fig. 10 shows variable parameters in the notch filter. In the table, f_s is the start frequency of compensation and f_e is the end frequency of compensation. In the case of switching of the filter during the robot motion, the vibration might be generated by discontinuous control input. In the low velocity motion, however, the discontinuous control input by switching does not affect the control performance because of the small variation.

Fig. 11 shows gain characteristics of the notch filter and $G_{al}(s)$, while Fig. 12 shows Nyquist diagrams of the feedback control system with the notch filter. In these figures, the characteristics change from light line to dark line according to the motor angular velocity. From the bottom figure in Fig. 11, the gain reduction under the target constraint of (5) (represented by broken line) can be achieved by applying the notch filter. From the Fig. 12,

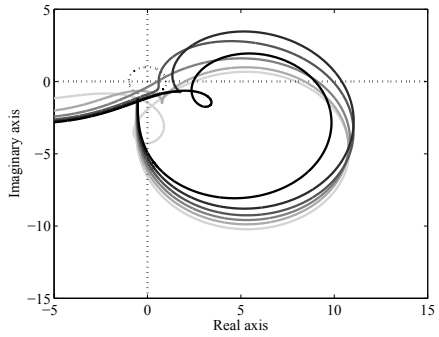

(a) Nyquist diagrams.

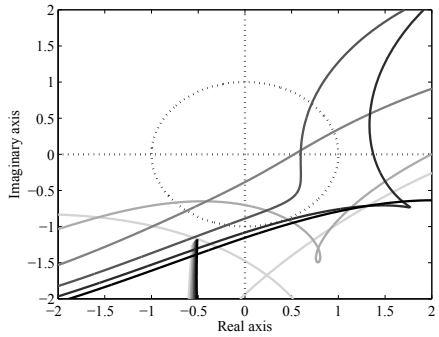

(b) Magnified nyquist diagrams.

Fig. 12. Nyquist diagrams for designed variable notch filter.

on the other hand, the sufficient system stability can be achieved in all motor angular velocity range.

5. EXPERIMENTAL VERIFICATIONS

5.1 Single Axis Motion

The proposed control approach has been verified by experiments for a single axis motion. The designed compensation has been implemented in a discrete manner by a bilinear transformation with the sampling time of $T_s = 250$ μs. Figs. 13 and 14 show experimental waveforms of acceleration response and the corresponding frequency analyses, where broken lines represent without the notch filter, solid lines represent with the notch filter, and horizontal dotted lines in upper figures represent the target specification. In these cases, the motor drives under the constant acceleration, while the references of other axes motor except for the driving axis are set as of zero. From these results, resonant vibrations can be suppressed, while the acceleration responses can be satisfied the target specification by applying the proposed controller.

5.2 Line Motion

Fig. 15 shows experimental waveforms in the actual line motion, where the upper figure shows the acceleration responses, the lower figure shows the frequency analyses, broken lines represent without the notch filter, solid lines represent with the notch filter, and horizontal dotted lines in upper figure represent the target specification. From this result, the vibration can be suppressed from 0.5 s to 2.0 s in the acceleration response, while the area of acceleration spectrum can be reduced 26 %.

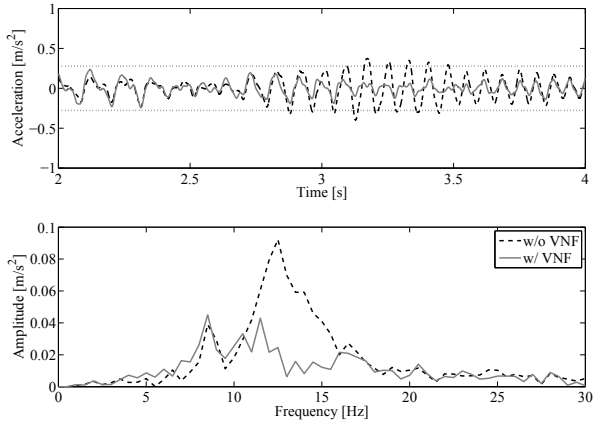

Fig. 13. Response waveforms of acceleration in 2nd axis motion with constant acceleration.

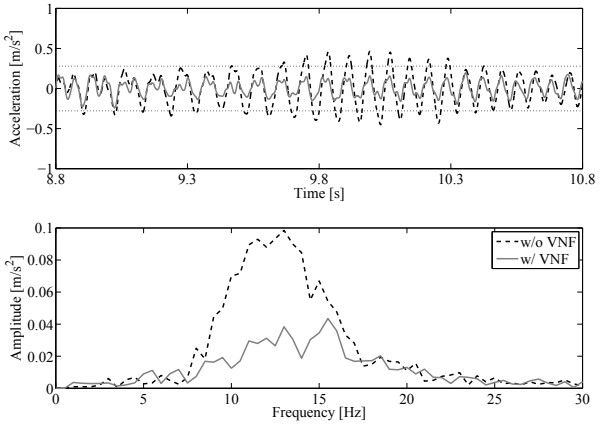

Fig. 14. Response waveforms of acceleration in 3rd axis motion with constant acceleration.

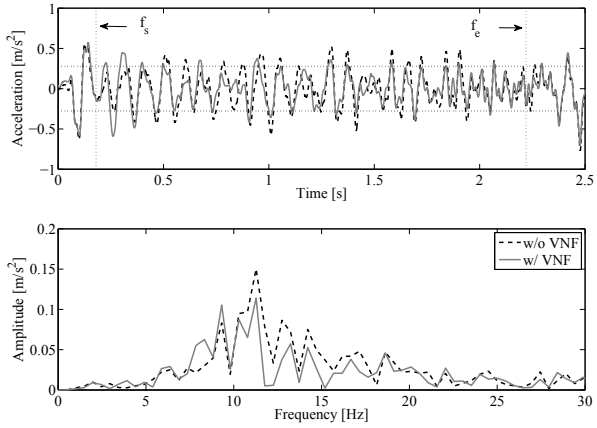

Fig. 15. Response waveforms of acceleration under line motion.

6. CONCLUSION

This paper presented a suppression approach for vibrations due to the synchronous component of HDG in the industrial robot system. Since the line motion with the low velocity drive was especially focused, the resonant vibration of the 2nd and 3rd axes was mathematically modeled and analyzed for the actual 6-axis industrial robot. Based on the simulator, the feedback compensator to suppress the vibration was designed from the viewpoint of loop-shaping, where the variable notch filter corresponding to the motor velocity was applied to reduce the sensitivity gain for the synchronous component as the disturbance. The proposed control has been verified by experiments using the actual 6-axis industrial robot.

REFERENCES

B. Bona, M. Indri, and N. Smaldone. Rapid Prototyping of a Model-Based Control With Friction Compensation for a Direct-Drive Robot. *IEEE/ASME Transactions on Mechatronics*, Vol.11, No.5, pp.576–584, 2006.

F.H. Ghorbel, P.S. Gandhi, and F. Altpeter. On the kinematic error in harmonic drive gears. *ASME J. Mech. Des.*, Vol.123, pp.90–97, 2001.

I. Godler, T. Ninomiya, and M. Horiuchi. Ripple Compensation for Torque Sensors Built into Harmonic Drives. *IEEE Transactions on Instrumentation and Measurement*, Vol.50, No.1, pp.117–122, 2001.

M. Iwasaki, M. Yamamoto, H. Hirai, Y. Okitsu, K. Sasaki, and T. Yajima. Modeling and Compensation for Angular Transmission Error of Harmonic Drive Gearings in High Precision Positioning. *Proc. of IEEE/ASME International Conference on Advanced Intelligent Mechatronics*, pp.662–667, 2009.

C.W. Kennedy and J.P. Desai. Modeling and control of the Mitsubishi PA-10 robot arm harmonic drive system. *IEEE/ASME Transactions on Mechatronics*, Vol.10, No.3, pp.263–274, 2005.

K. Khorasani. Adaptive Control of Flexible-Joint Robots. *IEEE Transactions on Automatic Control*, Vol.8, No.2, pp.250–267, 1992.

E-J. Kim, K. Seki, M. Iwasaki, and S-H. Lee. GA-Based Practical Auto-Tuning Technique for Industrial Robot Controller with System Identification. *IEEJ Journal of Industry Applications*, Vol.1, No.1, pp.62-69, 2012.

T. Miyazaki and K. Ohishi. Robust speed control system considering vibration suppression caused by angular transmission error of planetary gear. *IEEE/ASME Transactions on Mechatronics*, Vol.7, No.2, pp.235–244, 2002.

K. Seki, M. Iwasaki, M. Kawafuku, H. Hirai, and K. Yasuda. Adaptive Compensation for Reaction Force with Frequency Variation in Shaking Table Systems. *IEEE Transactions on Industrial Electronics*, Vol.56, No.10, pp.3864–3871, 2009.

M.W. Spong, K. Khorasani, and P.V. Kokotovic. An Integral Manifold Approach to the Feedback Control of Flexible Joint Robots. *IEEE Journal on Robotics and Automation*, Vol.3, No.4, pp.291–267, 1987.

M.W. Spong, S. Hutchinson, and M. Vidyasagar. *Robot Modeling and Control*. John Wiley and Sons, Inc., 2005.

T.D. Tuttle and W.P. Seering. A Nonlinear Model of a Harmonic Drive Gear Transmission. *IEEE Transactions on Robotics and Automation*, Vol.12, No.3, pp.368–374, 1996.

M. Yamamoto, M. Iwasaki, M. Kainuma, Y. Okitsu, K. Yuki, K. Sasaki, and T. Yajima. Compensation for Synchronous Component of Angular Transmission Errors in Harmonic Drive Gearings. *Proc. of International Workshop on Advanced Motion Control*, pp.361–365, 2010.